Report Bachelor Project Physics and Astronomy, size 15 EC

Conducted between:
02.04.2024 - 01.07.2024

Measuring the light absorption of VUV wavelengths as a function of pressure

AUTHOR	Dagmar Salomons
STUDENT ID	13981714
SUBMISSION DATE	01.07.2024
SUPERVISOR	Dr. Tina Pollmann
DAILY SUPERVISOR	Marjolein van Nuland-Troost
SECOND EXAMINER	Dr. Jory Sonneveld
INSTITUTE	Nikhef
UNIVERSITIES AND FACULTIES	Universiteit van Amsterdam, Faculteit der Natuurwetenschappen, Wiskunde en Informatica Vrije Universiteit Amsterdam, Faculteit der Bètawetenschappen

VU VRIJE UNIVERSITEIT AMSTERDAM | UNIVERSITY OF AMSTERDAM

Populair wetenschappelijke samenvatting

Sommige deeltjes in ons universum zijn heel moeilijk te detecteren. Deze deeltjes reageren niet met licht, waardoor wij speciale technieken nodig hebben om deze deeltjes waar te nemen. Neutrinos en donkere materie zijn dit soort moeilijk waar te nemen deeltjes. Neutrinos zijn elementaire deeltjes met bijzondere eigenschappen die we nog niet helemaal begrijpen. Donkere materie is materie die wij niet kunnen zien, maar door de zwaartekracht van deze deeltjes weten we dat ze bestaan. We weten nog niet precies waar donkere materie uit bestaat. Een van de theorieën stelt dat er een zwaar deeltje bestaat dat weinig interactie aangaat met zichtbare materie, het Weakly Interacting Massive Particle (WIMP).
Soms reageren Neutrinos en WIMPs wel met xenon of argon. Door grote detectoren te vullen met die elementen kunnen neutrinos en WIMPs gedetecteerd worden. Als zo'n deeltje met het xenon of argon reageert, dan komt er licht vrij. Dit licht willen onderzoekers graag meten, maar dan is het belangrijk om te begrijpen hoe het materiaal van de detector reageert op dat licht. VULCAN is een opstelling om de materialen van de detectoren te onderzoeken. Het licht dat vrijkomt in de detectoren heeft een specifieke golflengte. Door licht met dezelfde golflengte te creëren, kan onderzocht worden hoe het materiaal op het licht van de interacties in de detectoren reageert. De golflengtes van dit licht worden geabsorbeerd door zuurstof in de lucht. Om deze reden moeten de metingen van VULCAN in een vacuum gedaan worden.
In dit project heb ik metingen gedaan om te bepalen hoeveel licht er wordt geabsorbeerd als functie van de druk. Hiermee kunnen we bepalen hoe goed het vacuum in VULCAN moet zijn om metingen te doen. De metingen heb ik herhaald, maar daar kwam geen eenduidig resultaat uit. Er moeten dus meer metingen gedaan worden om te achterhalen waar dat door komt.

Abstract

In this project the light absorption of vacuum ultraviolet wavelengths as a function of pressure has been measured. This was done to determine the pressure requirements of the VULCAN setup. This setup is designed to measure the optical properties of materials used in dark matter and neutrino detectors. These detectors record the scintillation light resulting from dark matter or neutrino interactions inside the detectors. Xenon and argon are used inside these detectors and they produce scintillation light with a wavelength of 178 nm and 128 nm respectively. It is important to understand how the detector interacts with this light. A temperature sensor was installed in the VULCAN setup before the measurements were taken. The temperature sensor has been calibrated using a linear fit. Measurements were taken while the vacuum pump was turned on. The vacuum pump was turned off at a pressure of 10^{-4} mbar and another measurement was taken while the pressure climbed up to atmospheric pressure. Three wavelengths have been chosen for this project, 128 nm, 140 nm and 178 nm. The data with the vacuum pump on and off have been analysed separately. An exponential fit has been made to analyse the data. The absorption cross section exponents, -22 for a cross section of $10^{-22}\,\mathrm{m}^2$, of air (oxygen) have been extracted from the fit. The absorption cross section exponents are $-21.36(4)$ and $-20.25(2)$ for 128 nm, $-23.51(7)$ and $-21.13(15)$ for 178 nm, and $-20.80(3)$ and $-20.94(3)$ for 140 nm. The large difference between the found cross sections for the same wavelength indicates there could be another variable that was not considered in this project.

Table of contents

1 Introduction

1.1 Dark matter

In the nineteenth century astronomers already proposed the existence of undetected matter, based on its gravitational influence. Mathematician Friederich Bessel was the first, in 1844, to propose an undiscovered object to explain the proper motion of the stars Procyon and Sirius. Two years later a planet was proposed by two astronomers to explain the anomalies in the motion of Uranus. This planet was discovered and later called Neptune [1]. This proves the existence of previously unseen matter. Since then more evidence for the existence of undetected, dark matter has been found. There are several astrophysical observations to support the existence of dark matter, some of which are discussed in [2]. An important indication for the existence of dark matter were the flat rotation curves of galaxies [1]. Most of the mass is concentrated around the centre of the galaxy and after a certain radius the mass remains equal. It was expected that the rotational velocity of the matter in a galaxy increased with the radius as the enclosed matter increased. When the enclosed matter no longer increases with the radius, the rotational velocity should decrease with $r^{-1/2}$. Instead, the rotational curves were found to stay flat after the initial increase. This would indicate more matter is present than is to be expected from the luminosity. A few theories are proposed for dark matter, one of which is the Weakly Interacting Massive Particle (WIMP) [2].
This particle rarely interacts with ordinary matter, so it is hard to detect. One experiment designed to detect this particle is XENONnT. This is a dual-phase xenon time projection chamber (Xe TPC). This detector contains both liquid and gaseous xenon. Arrays of photo multipliers at the top and bottom of the detector detect the light from interactions with the xenon. When a WIMP interacts with the liquid xenon, the xenon is ionized. This interaction creates scintillation light, the S1 signal. The electron from the ionization will be pulled away due to the electric field inside the detector. This electron will produce a second photon when it reaches the gas phase, the S2 signal [2].

1.2 Neutrinos

Another weakly interacting particle is the neutrino, a neutral elementary particle. They were first proposed in 1930 by Pauli to explain the beta decay spectrum [3]. The electron emitted in the beta decay of a nucleus had a continuous spectrum instead of a single energy. This would violate the conservation of energy. Pauli suggested another neutral particle was emitted as well, the neutrino as it would later be called, which would have part of the energy. The neutrino was observed in 1953 [3]. Since then several properties of neutrinos have been observed, such as three neutrino flavours: ν_μ, ν_τ and ν_e. Neutrinos can change flavour as they travel. This is called neutrino oscillation [3].
The Deep Underground Neutrino Experiment (DUNE) is an experiment designed to measure these oscillations, in addition to proton decay and supernovae neutrinos. This experiment has a near and far detector to measure the neutrino oscillations. DUNE is a single-phase argon TPC. A neutrino interaction with argon creates scintillation light and charged particles. The scintillation light indicates the time of the interaction. On their track through the liquid argon, the charged particles create electrons by ionizing the argon. These electrons drift away due to the electric field and are recorded by wire planes. A 3D reconstruction of the track can be made

by combining the signals of the scintillation light and electrons recorded by the wire planes. [3].

1.3 Measuring optical properties of detector materials in the VUV

The scintillation light produced inside the dark matter and neutrino detectors interact with the detector materials. It is important to understand the interaction of the detector with the produced light. The optical properties of the materials are determined by reflectivity, transmittance and fluorescence measurements. The scintillation light produced by interactions with liquid xenon (LXe) or liquid argon (LAr) has a wavelength in the vacuum ultraviolet (VUV) range. These wavelengths get absorbed mostly by oxygen [4]. Therefore, the measurements to determine the optical properties have to be performed in a vacuum. The required pressure for these measurements has been estimated to be $1 \cdot 10^{-5}$ mbar [5]. In this project, the light absorption of vacuum ultraviolet wavelengths as a function of pressure will be measured. The scintillation light from the LXe and LAr experiments has wavelengths of 178 nm and 128 nm respectively. Therefore, these wavelengths will be the focus of this experiment. To verify the absorption spectrum of the light, which depends on the wavelength, a wavelength of 140 nm will also be measured. The transmittance of light through air has been calculated assuming only oxygen is responsible for the absorption of light. For a path-length of 0.3 m and a pressure of $1 \cdot 10^{-4}$ mbar, the transmittance at 128 nm (178 nm) is 99.999 79 % (99.999 73 %). The transmittance at 140 nm is 99.975 % under the same circumstances [5].
This experiment intends to confirm the calculations for the required pressure and determine if the difference in intensity at different wavelengths can be observed.

2 Theory of light absorption

The absorption of light can be described by the Beer-Lambert Law [4]:

$$I = I_0 e^{-\sigma N} \tag{1}$$

with I the intensity, I_0 the maximum intensity, σ the absorption cross section and N the number of particles. The number of particles depends on the density, which changes during the measurement due to the vacuum pump, and the distance. The density can be related to the pressure (P) according to the ideal gas law [5]:

$$\rho = \frac{0.2094MP}{RT} \tag{2}$$

with 0.2094 the percentage of oxygen in the air, M the molar mass of oxygen, R the gas constant and T the temperature.
The number of particles can be described by the following equation [5]:

$$N = \frac{0.2094PN_a d}{RT} \tag{3}$$

with N_a Avogadro's number and d the distance.

In air, the oxygen is responsible for the light absorption in the VUV wavelength range. The absorption cross section is strongly dependent on the wavelength, below 260 nm the absorption by oxygen becomes important [4]. Nitrogen has a much smaller cross section than oxygen for

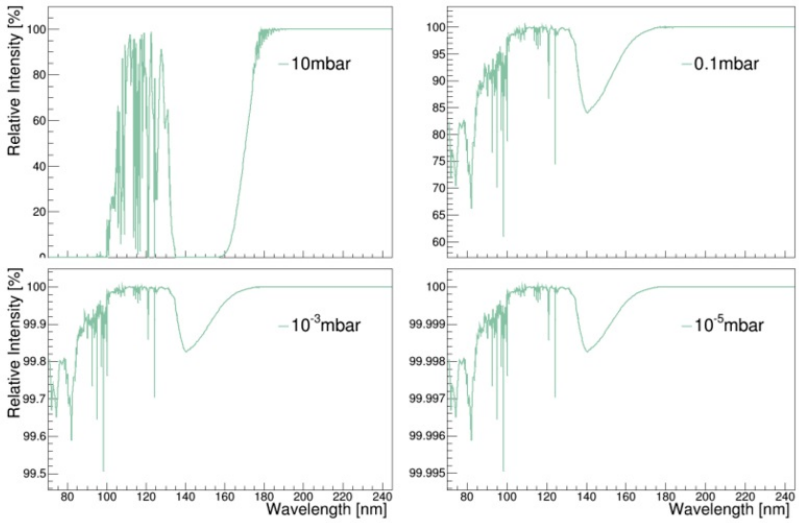

Figure 1: The transmittance of wavelengths in the range of 70 nm to 245 nm at different pressures. The y-axes in these plots change with the pressure.

wavelengths above 100 nm [4]. In this project, oxygen is assumed to be responsible for the absorption of light and nitrogen is ignored as it has a much smaller cross section. In figure 1 the transmittance at a distance of 0.3 m for wavelengths in the range 70 nm to 245 nm is shown at different pressures. At 10 mbar light is almost completely absorbed for most wavelengths below 180 nm and at 10^{-5} mbar light gets almost fully transmitted for all wavelengths. The cross sections for 128 nm, 140 nm and 178 nm are 10^{-23} m^2, 10^{-21} m^2 and 10^{-23} m^2 respectively [4].

3 Method

VULCAN stands for Vacuum Ultraviolet Light Characterisation At Nikhef. The optical properties of materials can be measured using this setup, with a focus on materials used in dark matter and neutrino experiments. The setup, experimental method and data analysis will be explained in this section.

3.1 VULCAN setup

A schematic version of the setup is shown in figure 2. The deuterium lamp creates a spectrum of wavelengths and a specific wavelength is chosen using the monochromator. The light enters the vacuum chamber and hits the sample of the studied material. SiPMs are installed to measure single photons being transmitted or reflected. The pressure and temperature is monitored as well. The SiPMs are operated with a bias voltage. Their signals are amplified before they are sent to a digitizer. The components of the setup will be explained in more detail in the next subsections.

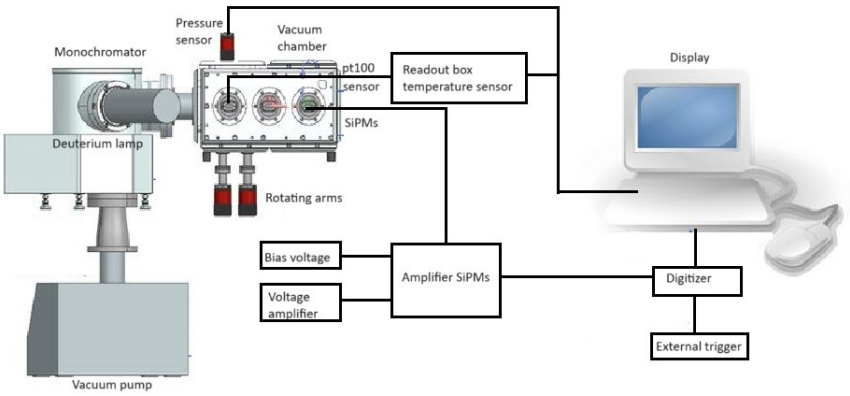

Figure 2: Schematic drawing of the VULCAN setup. This figure was taken from the DAQ page at the Nikhef wiki page [6] and modified to the current setup. A spectrum of light is created in the deuterium lamp. The monochromator is used to select one wavelength. In the vacuum chamber, the light hits the sample of a material. SiPMs are used to detect the photons being transmitted or reflected. The SiPM signal is amplified and sent to a digitizer. The pressure and temperature are monitored using a pt100 temperature sensor and a full-range pressure sensor.

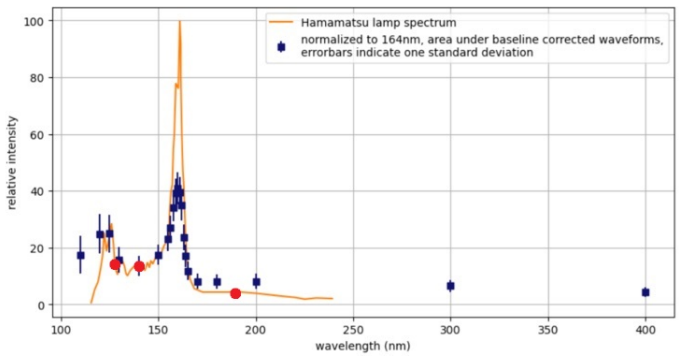

Figure 3: Intensity spectrum of the deuterium lamp. The intensity spectrum of the lamp has been measured before the start of this project by another student. The spectrum of the lamp provided by the manufacturer is compared to measurements of the light intensity. The intensity measurements have been corrected for the SiPM efficiency, which varies with wavelength. This graph has been taken from the Nikhef wiki page, see [7]. The red dots indicate the wavelengths that are being measured in this experiment: 128 nm, 140 nm and 178 nm.

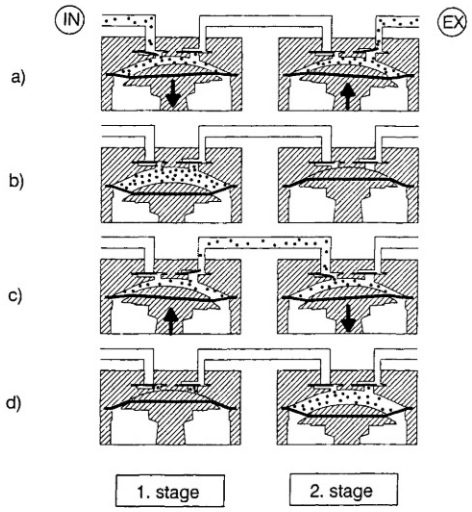

(a) The pumping cycle of a two stage diaphragm pump [12].

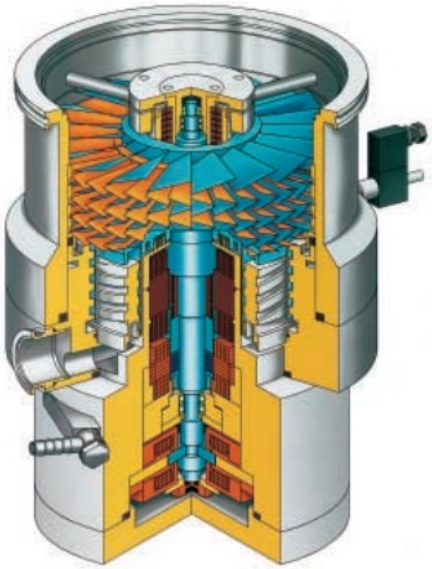

(b) Schematic view of the inside of a turbopump [13].

Figure 4: This figure shows the two kinds of vacuum pumps used in the VULCAN setup, a diaphragm and turbomolecular pump.

3.1.1 Deuterium lamp and monochromator

The light source is a Hamamatsu deuterium lamp (model L15094) with a magnesium fluoride window, which has an high transmittance for VUV wavelengths. This lamp creates a spectrum of wavelengths in the VUV range from 115 nm to 240 nm [8], though there is lower intensity light all the way to 400 nm. The intensity spectrum of the lamp has been measured before the start of this project, see figure 3. The wavelength can be selected with the monochromator (McPherson 234/302).
The monochromator has an aberration corrected Seya-Namioka design. The entrance and exit slits are fixed at a 64° angle [9]. The reflective grating inside the monochromator can be rotated to select a wavelength. The diffraction grating will split the incoming light into different wavelengths. The selected wavelength is directed towards the exit slit by rotating the grating. The groove density of the grating affects the dispersion of the light and the spectral range. The spectral resolution increases with the groove density, whereas the spectral range decreases [10] [11]. In this setup, a 1200 g/mm grating coated with $Al + MgF_2$ is used, which has a wavelength range up to 550 nm [9]. The entrance and exit slits can be adjusted in size to change the size of the beam. The entrance slit is mainly used to control the intensity of the light, while the exit slit is primarily used to adjust the accuracy of the selected wavelength.

3.1.2 Vacuum chamber and pump

The vacuum pump is connected to the monochromator and by extension to the vacuum chamber from IdealVac. The light enters the vacuum chamber through the monochromator and hits the sample. The sample holder can be rotated using rotating arms outside the chamber. The transmitted or reflected light is collected by the SiPMs. There are two SiPMs inside the holder, which can rotate around the sample. A pt100 temperature sensor is installed to monitor the

temperature during the measurement. The pressure sensor is connected to the vacuum chamber.

The vacuum pump consists of a backing pump and a turbopump from Pfeiffer, see figure 4. The backing pump is used to quickly create a low vacuum around 5 mbar [14]. Then the turbopump takes over to create a high vacuum. In this setup the backing pump is a diaphragm pump, see figure 4a for the operating principle of a diaphragm pump. A diaphragm pump has two valves, the inlet and outlet valve. These valves are connected to the pumping chamber, where a diaphragm is moved up and down. When the diaphragm is moved down, the volume in the pumping chamber increases and the inlet valve opens due to the pressure difference between the pumping chamber and the volume where a vacuum has to be created. When the pumping chamber is at a maximum, the pressures are equal and the inlet valve is closed. Then the diaphragm is moved up and the outlet valve opens. Both valves are closed when the pumping chamber has the smallest volume. In the case of connected pumps, the outlet valve is connected to the inlet valve of the second pump. Connecting multiple pumps can create a better vacuum. The achievable vacuum is limited by the remaining gas inside the pumping chamber at the lowest volume [12]. When the highest achievable vacuum is created, the turbomolecular pump, or turbopump, takes over.
The turbopump consists of alternating disks of rotating and stationary blades, see figure 4b. The blades of the rotating and stationary disks are installed in mirror image. The gas molecules will be hit by a rotating blade and the momentum of the blade is transferred to the molecules. The direction of the molecules is changed and directed toward the stationary disk. The stationary blades ensure the molecules will move downward to the next rotating disk. The random motion of the molecules is transformed to a directed motion. This removes molecules from the chamber connected to the pump, creating a vacuum. This method only works if the blades hit the molecules more frequently than the molecules collide with each other, creating a random motion again. Therefore, this pump cannot operate at higher pressures. Too many molecules will collide with each other, eliminating the directed motion that is created [15].

3.1.3 SiPM

The silicon photo multipliers (SiPM) used in this setup are the VUV-MPCC 4th generation from Hamamatsu. These SiPMs are suitable to detect scintillation light from liquid xenon or argon [16]. SiPMs are single-photon avalanche diodes [17]. These diodes are a 2D array of avalanche photo diodes (ADP) connected in parallel. The ADPs can only distinguish between presence and absence of photons, not the number of photons incident on the ADP. By connecting the ADPs in parallel, multiple photons can be detected [18]. A diode has a p-n region, the connection between a positive and negative doped material. These materials have an excess in holes and electrons respectively. When they are connected, the electrons and holes recombine at the junction. The positive and negative ions of the doped material will create an electric field at the junction. The electrons and holes cannot cross this electric field and a depletion region is created without charge carriers. A reverse bias increases the depletion region and therefore the electric field. When a photon hits the depletion region, an electron-hole pair is created. The electron and hole drift away from each other due to the electric field. If this field is strong enough, the charge carriers gain enough speed to be able to ionize an ion in the depletion region. This will create another electron-hole pair and an avalanche is created. The breakdown voltage is the voltage at which this effect can take place. The diodes operate above

their breakdown voltage, in Geiger mode, so each photon creates an avalanche and a detectable voltage is generated. After this photon detection, the avalanche has to be stopped to allow for the next detection. This is called quenching [19]. The voltage has to drop below the breakdown voltage, so that all the build-up charge inside the p-n junction can clear out and the avalanche is stopped. Then the bias voltage can be restored and the next photon can be detected [20].

An electron-hole pair can be created by thermal excitation instead of a photon [19]. This will start an avalanche as well, which is indistinguishable from a photon induced avalanche. This noise is called dark count. These dark counts are strongly dependent on the temperature. In a previous project an exponential dependence on the temperature has been found [21].

3.1.4 Slow control

The slow control consists of the pressure and temperature sensor. This is called slow control, because the SiPMs are read out with a sampling rate O(ns), while these sensors are read out with a much slower sampling rate of only O(s). The pressure sensor is a Pfeiffer full range pressure gauge (MPT 200), with a range of $5 \cdot 10^{-9}$ mbar to 1000 mbar [22]. This model has two kinds of sensors built in, the Pirani and Cold Cathode sensors. The Pirani sensor is used for higher pressures. Around $1 \cdot 10^{-3}$ mbar the gauge switches to the Cold Cathode sensor [22]. These two sensors rely on different methods to measure the pressure.

The Pirani sensor uses the thermal conductivity of gasses to measure the pressure. This sensor has a spiral coil filament that is heated to a constant temperature [23]. The gas molecules around the filament will dissipate heat through thermal conductivity. The number of gas molecules, and therefore the thermal conductivity, increases linearly with the pressure [24]. More heat will be dissipated as the pressure increases. As a result, the current through the filament has to increase as the pressure increases to keep the filament at a constant temperature. Therefore, the current is a measure of pressure. The lower limit for this type of sensor is caused by heat losses other than thermal conduction through the gas. Heat is lost through thermal radiation and thermal conduction through the suspension of the filament, which are independent of the pressure. At the lower limit, these heat losses exceed the heat loss through the gas and the current is no longer pressure dependent [24]. The upper limit is caused by the saturation of the thermal conduction through the gas. At the upper limit, the numerous gas molecules will collide with each other so frequently the thermal conduction gets saturated [24].

The Cold Cathode sensor is an ionization gauge. In these gauges a high voltage is applied between a cathode and an electrode via a resistor connected in series. There are multiple designs for cold cathode gauges. Pfeiffer chose an inverse magnetron design with a metal pin, the anode, surrounded by a cylindrical cathode [23], see figure 5. Electrons will be emitted from the cathode through field emission [23]. The electrons will ionize gas molecules while moving from the cathode to the anode, producing an electron and a cation. The cation will move to the cathode and produce an ion current. The electron is able to ionize another gas molecule. The number of produced cations will increase with the number of gas molecules, so the ion current is a measure of pressure. The initial electron current from the field emission is small, so the chance of ionizing a gas molecule would be very small if the electrons moved directly from the cathode to the anode. To increase the path length the electrons have to travel, a magnetic field is applied such that the electrons move in spirals to the anode. This will allow for more

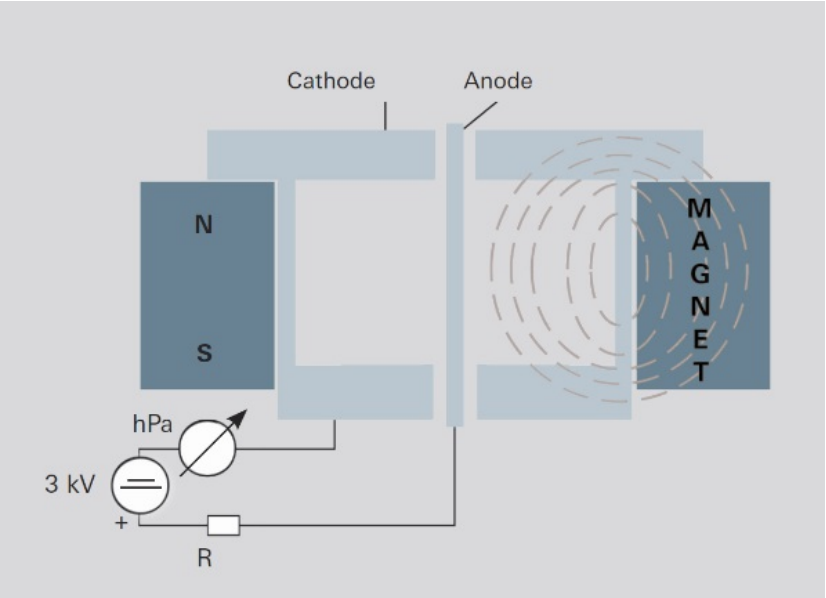

Figure 5: Schematic drawing of the inverse magnetron cold cathode pressure gauge used by Pfeiffer. This figure was taken from [23].

ionizations. At low pressures, there will not be enough electrons created from the ionization to maintain the electron current [23] [25]. The ion current will become too small to detect. The introduction of the magnetic field in the cold cathode gauge has increased the sensitivity due to the longer path of the electrons [23]. The upper limit for the pressure is set by the series resistor. The ion current will increase with the pressure, until it is limited by the series resistor [25].
The temperature sensor used in this setup is a pt100, a type of RTD (Resistance Temperature Detector). The pt stands for the material used inside the sensor, platinum, and 100 is the resistance in Ω at 0 °C. The resistance of these sensors are temperature dependent, and in the case of platinum this dependence is linear [26]. The pt100 in this setup has a temperature coefficient of $+0.3916\,\Omega\,\mathrm{K}^{-1}$ [27]. Due to the linear dependence, it is possible to calculate the temperature if the resistance is measured.
There are multiple ways to connect wires to the pt100 for the read out. In this experiment, the sensor was installed using a two-wire connection. The used wires are Kapton-coated copper wires, which are suitable for vacuum applications. A VGA cable was used to connect the vacuum chamber to the readout box for the pt100. This two-wire connection adds an extra resistance of the wires and the cable to the measurement of the pt100 resistance element. Therefore it is necessary to perform a calibration of the sensor [28]. This connection was chosen, because the readout box made for the temperature sensor was designed for a two-wire connection. The installation and calibration of the pt100 were a part of this project.

3.1.5 DAQ

The system to read out the SiPMs consists of an external trigger, a bias voltage for the SiPMs, a voltage for the amplifier and a digitizer. The digitizer converts the signal from the SiPMs

to binary code, so the computer can read the signal. The external trigger controls when the digitizer takes data and is set to 1000 Hz. The external trigger ensures the digitizer does not get too busy, because it will stop saving data at that point. The bias voltage for the SiPMs is set around 56 V. The breakdown voltage of the SiPMs is 53(5) V. Measuring the exact breakdown voltage is outside the scope of this project, so a breakdown voltage of 53 V is assumed. A voltage of 7 V is sent to the amplifier of the SiPM signal. The signal from the SiPMs is very small, so this signal has to be amplified. Two SiPMs connected to different read-out boards have been used, because the best performing board had not been identified yet so several were being tested.

3.2 Temperature sensor calibration

The pt100 was calibrated using an Isotech Europa 4520 Temperature Calibrator. It has a small container that can be filled with multiple liquids depending on the temperature range needed for the calibration. The temperature of the liquid inside the container can be controlled. An accurate calibration sensor will give a precise temperature measurement and the pt100 will give the corresponding voltage. In this experiment the temperature would remain around room temperature, so demineralized water with a temperature range of 0 °C to 100 °C was used. The water is continuously stirred to create a water bath of uniform temperature. The calibration sensor and the pt100 are placed inside the water bath. The temperatures were set at 15 °C, 20 °C, 25 °C, 30 °C, 40 °C and 50 °C. These temperatures were chosen, because the calibration is focused on temperatures around room temperature. The last two temperatures were chosen to get a larger range. The calibration sensor will measure the temperature with an error of 7/1000 °C. The readout box that was designed to read the temperature measures a voltage instead of the resistance. So, instead of converting resistance to temperature, the voltage is converted to temperature using the same linear dependence. The calibration of the temperature sensor will be analysed using a linear fit:

$$T = a \cdot V + b \tag{4}$$

with T the temperature, V the voltage and a, b constants provided by the fit.

3.3 Digitisation of the analogue signals

The SiPMs are positioned in the light beam using an oscilloscope. The SiPMs were rotated until the oscilloscope showed a strong signal. The sizes of the opening and exit slit were also determined using the oscilloscope. The lamp spectrum has a peak in intensity at 160 nm and the lowest intensity after 170 nm, see figure 3. The slit size has been chosen such that the signal of the SiPMs has significant results at both intensities. The signal from one photon takes about 160 ns to come back to baseline. If the rate of photons is too high, individual signals can no longer be separated, see figure 6. The sizes of the slits have been chosen such that there is still a baseline visible at 160 nm and there is enough light measured at 140 nm to exceed the dark count rate. The opening slit was set to 0.06 mm and the exit slit was set to 0.1 mm. The size of the exit slit is an upper limit for the size, because the exit slit cannot open all the way. The two SiPMs used in this experiment are positioned next to each other in the holder. Channel 1 was positioned in the middle of the light beam.

Unlike the pressure and temperature measurements, the SiPM runs are not continuous throughout the entire measurement. For the first 15 minutes, runs of 30 s are started continuously. The pressure is changing quickly during this time. Subsequently, 30 s runs are started for 2 minutes at random times when the pressure has changed. The vacuum pump cannot be set to a fixed pressure, so the measurements are done while the pressure is changing. The vacuum pump will be turned off after the pressure has come down to 10^{-4} mbar. While the vacuum pump is off and the pressure is climbing to atmospheric pressure, 30 s SiPM runs are started continuously. After the pressure stops rising, the vent on the vacuum chamber is opened to allow the pressure to go up to atmospheric pressure. This method was used for both the dark count measurements and the measurements with light. For the dark count measurements, the lamp was turned off. After the dark count measurement was taken, the lamp was turned on and set to the right wavelength. Before each measurement with light, a dark count measurement was taken to ensure similar circumstances. These measurements were done for 128 nm, 140 nm and 178 nm, with a bias voltage for the SiPMs of 56.32 V, 56.31 V and 56.31 V at the time of the measurement.

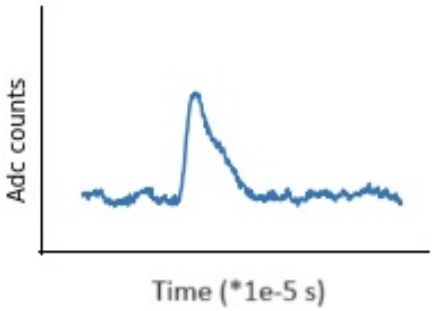

Figure 6: This is the trace of 1 photon taken from channel 1. There is a sharp peak when a photon is detected, which comes back to the baseline in about 160 ns.

3.4 Data analysis

The SiPM data consists of records, each 220 ns long. The zeros generated by the digitizer are deleted from the data. There are two methods of analysing the SiPM data. The data will show peaks when a photon is registered. The first method is to count the number of peaks, but higher or overlapping peaks due to multiple photons will not be recognized. The second method is to integrate the area under the peaks. This method is used in this report. The area under the peaks is divided by the area of a one-photon peak. Designing the algorithm to integrate the area under the peaks was not a part of this project, but I have made a small adjustment to correct the baseline.

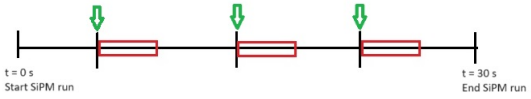

Figure 7: Visual representation of the data analysis. The green arrows indicate a pressure measurement and the red rectangles indicate the records of the SiPM data that are read.

The SiPM, temperature and pressure data has to be correlated in time. The temperature and pressure is measured every few seconds, so there are multiple measurements in one 30 second run from the SiPMs. For each pressure measurement, the corresponding temperature and records in the SiPM data are read. For every data point 5000 records will be read. These records are analysed using the integration method. See figure 7 for a visual representation of the analysis.

For the dark counts the temperatures are combined in bins of 0.6 °C, because the calibration

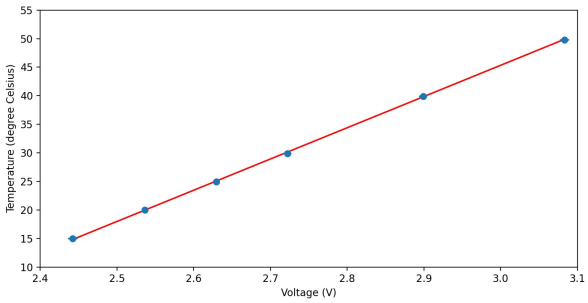

Figure 8: The linear fit of the temperature calibration of channel 0. The temperature is on the y-axis and the voltage on the x-axis. The constants a and b from the fit are 54.73(31) and −118.84(84).

of the pt100 showed an error of 0.3 °C. The average counts per bin are calculated and used as the dark counts for that temperature range. For the measurements with light, the dark counts are subtracted from the total counts. The counts are converted to the count rate in Hz.
The error on the counts follows Poissonian statistics. The errors on the count rate are calculated using the following equation:

$$\Delta R = \frac{\sqrt{N}}{\delta t} \tag{5}$$

with N the number of counts and δt the lifetime of the measurement.
The binning of the temperature changes the error calculation, so the error on the dark count rate is calculated as follows:

$$\Delta R_{dc} = \frac{\sqrt{(\sum N_i)}}{\delta t} \tag{6}$$

with N_i the number of counts of each measurement in the temperature bin and δt the lifetime of the measurement. The lifetime of the measurement is the combined lifetime of all measurements inside the temperature bin.
The error on the corrected count rate combines these two errors using error propagation:

$$\Delta R_{corrected} = \sqrt{(\Delta R)^2 + (\Delta R_{dc})^2} \tag{7}$$

4 Results

The temperature calibration was performed for the 8 different channels separately. The temperature measured by the calibration sensor was 14.99 °C, 19.96 °C, 24.94 °C, 29.90 °C, 39.91 °C and 49.81 °C. The voltage of the pt100 is plotted against the temperature and a linear fit has been made, see figure 8 for the graph of channel 0. The fits for the other channels look similar. The constants a and b have been extracted from the fit for each channel. The value of a is 54.73(31), 54.27(29), 54.62(14), 54.68(23), 54.59(27), 54.60(24), 54.61(27) and 54.60(25) and the value for b is −118.8(8), −118.6(8), −117.9(4), −118.9(6), −118.9(7), −118.6(6), −118.4(7) and −118.7(7) for channel 0 to 7 respectively.

Figure 9 shows the raw data of a dark count measurement produced by the digitizer. The y-axis shows the ADC counts and the x-axis is a randomly generated timescale. The first 40 µs of useful data is plotted. The two channels show different baselines and peak heights. This is due to the different measuring channels with different gains.

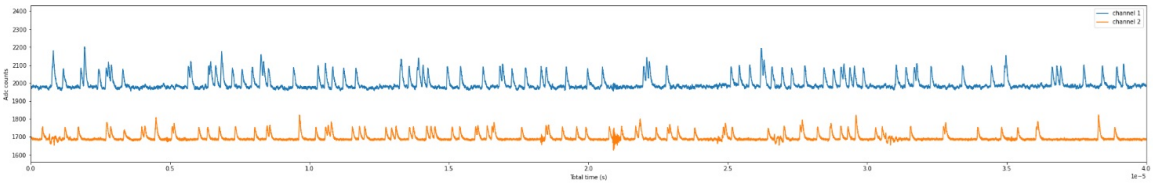

Figure 9: This figure shows the first 40 µs of data from channel 1 and 2. The time on the x-axis is a generated timescale and does not represent the actual time passed during the measurement. The y-axis shows the ADC counts. The two channels have a different baseline and peak height. The area under the peaks is calculated to determine the number of photons.

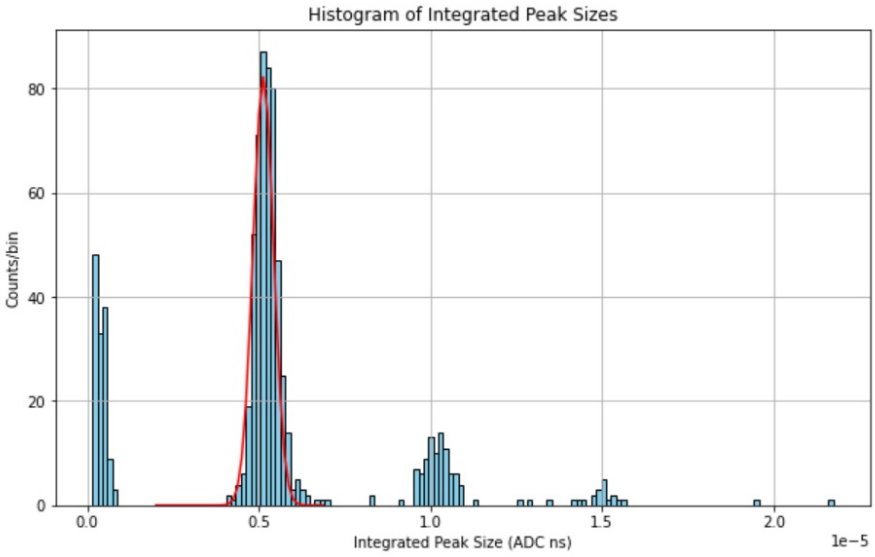

Figure 10: This figure shows a histogram of the area under the peaks. There is a peak around 0, which is the area of small peaks in the baseline. The highest peak represents the area of 1 photon, the next peak the area of 2 photons and so on. The red line is a Gaussian fit of the frequency and area. The centre of the Gaussian fit is used as the area of 1 photon.

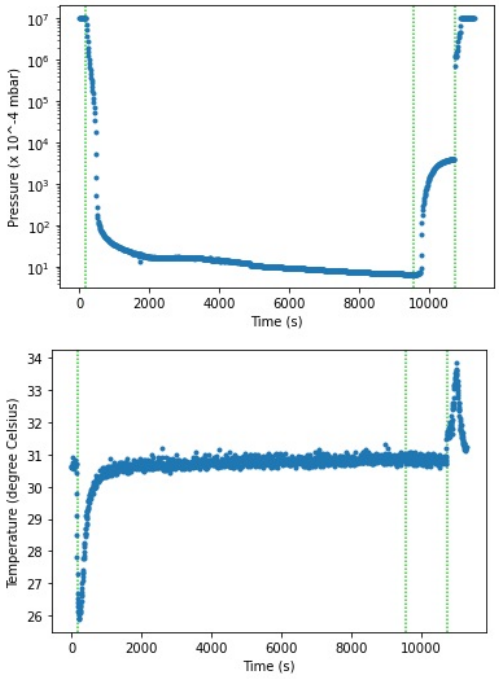

Figure 11: This figure shows the temperature and pressure measurements. The x-axis represents the time. The top graph shows the pressure and the bottom graph shows the temperature. The y-axis for the pressure is a logarithmic scale. In these graphs the starting time for both measurements are the same. The temperature decreases when the pressure decreases fast, and increases when the pressure increases fast.

The raw data of the dark count measurement was analysed by integrating the area under the peaks. This would provide the area for the peak created by one photon. The dark count measurements were used for this, because the one-photon peaks are most likely in these measurements. The area of the peaks are calculated and plotted in a histogram. The histogram for channel 2 of the raw data shown in figure 9, is shown in figure 10. The area is shown on the x-axis and the counts per bin on the y-axis. A peak in counts per bin is visible around an area of 0 ADC ns. These peaks are ignored as they are most likely caused by outliers in the baseline counted as peaks. The one-photon peaks will have the highest counts per bin. A Gaussian fit is made for the highest peak and the centre is used as the area for one photon. The other peaks represent one-, two- and three-photons, so they should be evenly spaced. Channel 1 and 2 are analysed separately, because they are connected to different boards. The area for one photon for channel 1 and 2 is $8.95 \cdot 10^{-6}$ ADC $\cdot$ ns and $5.12 \cdot 10^{-6}$ ADC $\cdot$ ns respectively.

The pressure and temperature graphs of the dark count measurement taken before the measurement of 140 nm are shown in figure 11. These graphs look equivalent for all other measurements. The time is on the x-axis and the pressure ($\cdot 10^{-4}$ mbar) and temperature (°C) on the y-axis. The pressure is on a logarithmic scale. The green dashed lines represent from left to right the time the vacuum pump was turned on, the pump was turned off and the vent-valve was opened. The decrease and increase in temperature corresponds to a quick drop and rise in pressure respectively. The jump in the pressure graph is caused by the venting. The temperature remains the same throughout the measurements as long as the pressure is changing slowly.

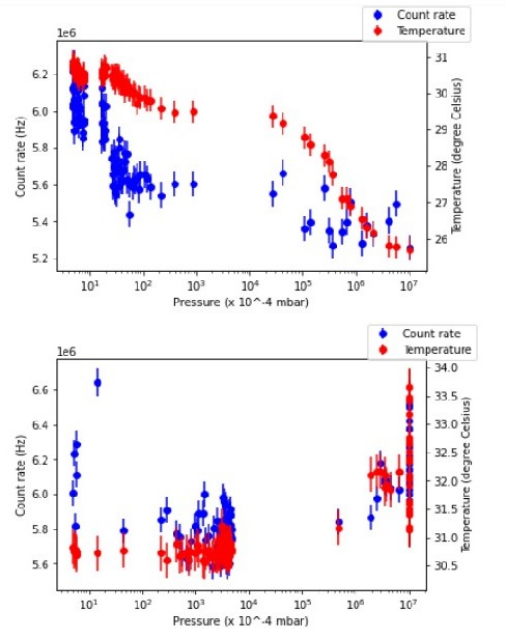

Figure 12: This figure shows the count rate and the temperature as a function of pressure for a dark count measurement. The blue points are the count rate and the red points are the temperature. The pressure axis has a logarithmic scale. The top graph shows the data when the vacuum pump is turned on, the bottom graph shows the data when the vacuum pump is turned off.

The count rate and temperature for the dark count measurement taken before the measurement of 128 nm is shown in figure 12. The measurement is split into two parts, the part where the vacuum pump is turned on and the part were it is turned off. The top graph shows the data with the pump on and the bottom graph with the pump off. The blue data points are the count rate and the red points are the temperature. The count rate rises with the temperature.

The uncorrected count rate and the temperature is shown in the graphs of figure 13. This is data from measurements with light at three different wavelengths: 128 nm, 178 nm and 140 nm. These graphs are split into two parts the same way as figure 12. The blue points represent the count rate and the red points the temperature. These count rates have to be corrected for the temperature dependent dark counts. These graphs are shown in figure 14. The temperature is no longer shown since this dependence is corrected for with the dark counts. The count rates are shown with an exponential fit of equation 1. The distance is set at 0.18 m. Different fits are made for the top and bottom graphs. The cross sections will be reported as the exponent of the cross section, so a cross section of $10^{-22}\,\mathrm{m}^2$ will be represented as -22. The exponent is given for a cross section with unit m^2. The maximum intensity and the cross sections are extracted from the fit. The absorption cross section exponents are $-21.36(4)$ and $-20.25(2)$ for 128 nm, $-23.51(7)$ and $-21.13(15)$ for 178 nm, and $-20.80(3)$ and $-20.94(3)$ for 140 nm.

The count rate for 178 nm is lower than the count rates of the other two wavelengths. This is due to the intensity spectrum of the lamp, see figure 3. The maximum count rates are 3.53(2) MHz and 3.49(8) MHz for 128 nm, 1.34(2) Hz and 1.29(10) Hz for 178 nm, and 5.97(2) MHz and 5.67(5) MHz for 140 nm.

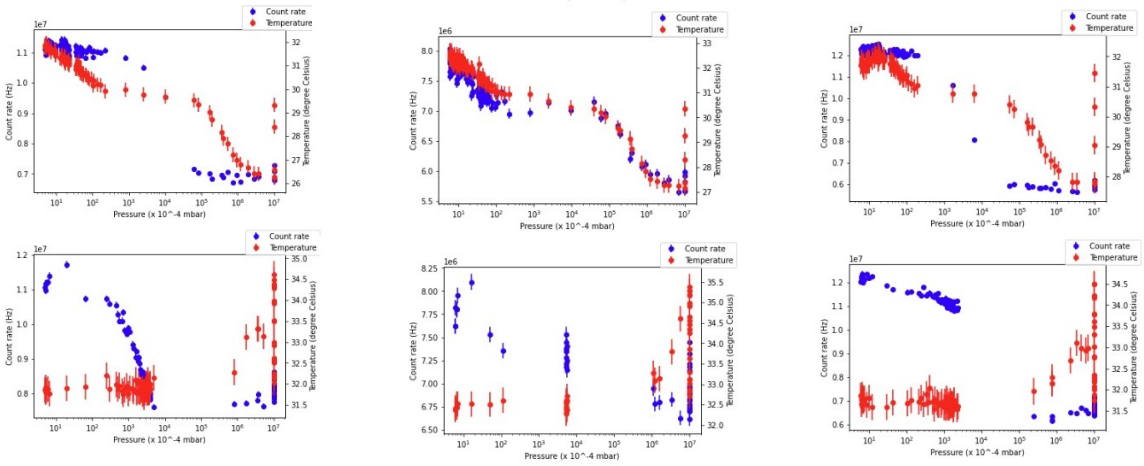

(a) wavelength = 128 nm (b) wavelength = 178 nm (c) wavelength = 140 nm

Figure 13: This figure shows the count rate and the temperature as a function of pressure. The blue points are the count rate and the red points are the temperature. The pressure axis has a logarithmic scale. The top graphs show the data when the vacuum pump is turned on, the bottom graphs show the data when the vacuum pump is turned off.

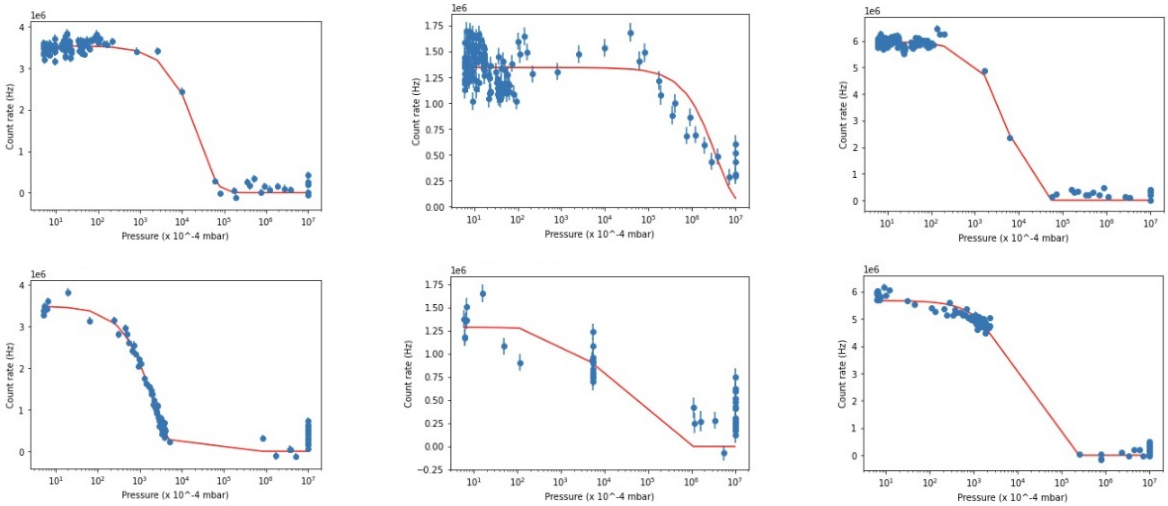

(a) wavelength = 128 nm (b) wavelength = 178 nm (c) wavelength = 140 nm

Figure 14: This figure shows the corrected count rates as a function of pressure and an exponential fit through the data points. The graphs are split again in the data when the vacuum pump is turned on (top graph) and off (bottom graph). The top and bottom graphs get different results for the maximum intensity and cross section.

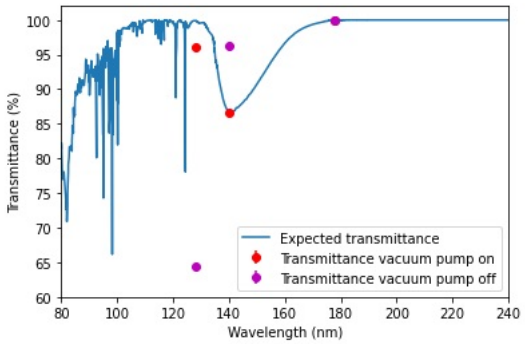

Figure 15: The graph from figure 1 is plotted again for a pressure of 0.1 mbar. The distance is 0.18 m and the average temperature of the measurements was taken at 31.5 °C. The cross sections found in the fit are used to calculate the transmittance for the measurements. The data points are normalised to the expected value for 178 nm, so the purple and red dot are at the same value for this wavelength. This graph shows the ratio between the measured data points.

The transmittance was calculated using the maximum intensity from the fit. The error on the transmittance is:

$$\Delta t = t \cdot \sqrt{\left(\frac{\Delta I}{I}\right)^2 + \left(\frac{\Delta I_0}{I_0}\right)^2} \tag{8}$$

with t the transmittance, ΔI the error on the corrected count rate, I the corrected count rate, ΔI_0 the error on the maximum count rate as given by the fit and I_0 the maximum count rate. The transmittance is almost 100 % at the lowest pressure. The errors on the transmittance are in the order of a few percent, which is too large to see the expected intensity difference at 140 nm at low pressures. The transmittance graphs are the same shape as the graphs with the count rate, so they will not be shown in the results section. See the appendix for the transmittance graphs.
Figure 15 shows the ratio of the transmittance between the data points. The transmittance is plotted for different wavelengths at a pressure of 0.1 mbar, a distance of 0.18 m and an average temperature of 31.5 °C. The data points are calculated by using the cross section from the fit. They are normalised to the expected value at 178 nm to see the ratio between the data points instead of the exact value. The error on the transmittance is calculated differently from equation 8, because the result from the fit was used. The following equation resulting from error propagation was used:

$$\Delta t = \sqrt{(-Ne^{-\sigma N} \cdot \Delta\sigma)^2} \tag{9}$$

with N the number of particles, see equation 3, σ the absorption cross section and $\Delta\sigma$ the error on the cross section. The error on the cross section was calculated by taking the absolute value of the difference between σ and $\sigma + / - \Delta\sigma$. The largest difference was used as the error on the cross section.
Figure 15 shows that the ratio between the data points when the vacuum pump is on (red data points) is close to the expected ratio. The ratio between the other data points does not match the expected ratio.

5 Discussion and conclusion

The temperature difference in figure 11 can be explained with adiabatic compression [29]:

$$VT^{f/2} = constant \tag{10}$$

with V the volume, T the temperature and f the degrees of freedom. The degrees of freedom are a constant throughout the measurement. The volume is inversely proportional to the density. Decreasing the density by pumping out gas molecules is equivalent to increasing the volume while keeping the same number of molecules. While the vacuum pump is decreasing the density, the temperature has to decrease as well as long as equation 10 holds. This is only true for adiabatic compression or expansion, or a quick decrease or increase in pressure. This is the reason the temperature changes during the measurement. The vacuum chamber is not thermally isolated, so when the change in pressure slows down the gas inside the vacuum chamber gets in thermal equilibrium with the room outside the vacuum chamber.

The measurement at 178 nm has an unexpected shape, with a small peak between 10^{-4} mbar and 10^{-5} mbar. The dark count corrections are done with a fairly wide temperature range to calculate the average dark counts. This measurement has a lower intensity and might be affected more by the uncertainty in this method. The bottom graph has a lot of data points around the same pressure with a different intensity. This measurement was taken while the vacuum pump was off, so the pressure should have changed continuously. It might be that the pressure sensor was not correctly read out during this measurement.
The cross sections for the different wavelengths found in the fit are different when the pressure pump is on and off. This difference was not expected, because there should be no difference in the light absorption whether the vacuum pump is on or off. It is possible the composition of the gas changes when the vacuum pump is turned off. The gas molecules that enter the vacuum chamber might not have the same composition as the air. Most of the air consists of nitrogen, which has a much smaller absorption cross section than oxygen in this wavelength range [4]. If oxygen were to enter the vacuum chamber at a higher rate than nitrogen, the absorption rate will increase. However, for 128 nm and 178 nm the difference between both cross sections is an order of magnitude or more. It is unlikely this is solely caused by a change in the oxygen concentration. More measurements would have to be taken to determine if this change in cross section happens at other wavelengths as well, since 140 nm does have two cross sections in the same order of magnitude.
Figure 15 shows the ratios between the data points when the vacuum pump is on (red) or off (purple). The data points when the vacuum pump is on are close to the expected values. However, the ratio between the data points when the vacuum pump is turned off does not match the expected ratio. This is another indication there might be a wavelength dependent variable that is not considered in this project. To confirm or refute this, the measurements would have to be repeated and more wavelengths should be measured. The errors on the transmittance calculated from the errors given by the fit are too small to be seen on the plot. It is possible the fit underestimated the errors, so the fit was made again for 128 nm with different ranges for the data to see the effect of variations in the data points. The fit was made by excluding a few data points at the highest or lowest pressures, while making sure the original shape of the data remained the same. The cross section was fitted again and compared to the original cross section. For all ranges of data tested the cross section remained within the error of the original

cross section.

In future experiments, the sample might be cooled down to temperatures below 0 °C. The calibration for the pt100 was performed with a focus on temperatures around room temperature. The calibration should still be valid, since the relationship between the voltage and the temperature is linear for this type of temperature sensor. However, this does not hold for all temperatures. It might be necessary to do another calibration for lower temperatures to check if the linear relationship still holds.
These measurements were taken at an average temperature of 31.5 °C. The dark count dependence on temperature is exponential, so performing measurements at lower temperatures would significantly decrease the dark count rate and the errors.
The vent valve was opened as soon as the pressure started increasing very slowly to let the pressure rise to atmospheric pressure. This happens at the pressure where the transmittance decreases quickly, so it is important to have many data points in that range. If it is possible to let the pressure rise slightly more than was done in these measurements, the fit would be more accurate.

The purpose of this project was to verify the calculations for the pressure requirements. In addition, the absorption difference between different wavelengths was investigated. The errors on the measurements are too large to differentiate between the small absorption differences for low pressures. The data is described by equation 1. The found cross sections are used to verify the calculations. For 140 nm the found cross section is in agreement with the literature. One cross section for 178 nm is in agreement with the literature, the other is off by two orders of magnitude. The cross sections found for 128 nm are off by about two orders of magnitude. The difference between the two found cross sections for each wavelength indicates there might be another variable that is not taken into account in this project.

6 Acknowledgements

I would like to thank the dark matter group for having me. A special thanks to Tina Pollmann and Marjolein van Nuland-Troost for their guidance throughout this project and always being available for questions. Also, I would like to thank Vikas Gupta and Corryenne Groen for their help with getting to know the setup.

References

[1] G. Bertone, D. Hooper, History of dark matter, *Reviews of Modern Physics* **90**, 045002 (2018).

[2] P. Gaemers, Electronic recoils in XENONnT, Ph.D. thesis, Universiteit van Amsterdam (2024).

[3] L. Camilleri, *Particle Physics Reference Library: Volume 2: Detectors for Particles and Radiation*, C. W. Fabjan, H. Schopper, eds. (Springer International Publishing, Cham, 2020), chap. Neutrino Detectors, pp. 337–382.

[4] R. E. Huffman, Absorption cross-sections of atmospheric gases for use in aeronomy, *Canadian Journal of Chemistry* **47**, 1823 (1969).

[5] VUV group Nikhef, Detailed setup description. https://wiki.nikhef.nl/vuv/Detailed_setup_description, Accessed at 07.06.2024.

[6] VUV group Nikhef, DAQ. https://wiki.nikhef.nl/vuv/DAQ, Accessed at 07.06.2024.

[7] VUV group Nikhef, Lamp spectrum measurement. https://wiki.nikhef.nl/vuv/Lamp_spectrum_measurement, Accessed at 10.06.2024.

[8] Hamamatsu, VUV light source unit L15094. https://www.hamamatsu.com/eu/en/product/manufacturing-support-systems/electrostatic-remover/vuv-ionizer/L15094.html, Accessed at 07.06.2024.

[9] McPherson, 234/302 Data Sheet. https://www.mcphersoninc.com/pdf/234302.pdf, Accessed at 08.06.2024.

[10] Edinburgh instruments, Grating Selection for Ramen Spectroscopy. https://www.edinst.com/technical-note-grating-selection-for-raman-spectroscopy/#:~:text=Gratings%20have%20a%20defined%20groove,a%20150%20gr%2Fmm%20grating., Accessed at 08.06.2024.

[11] Newport Corporation, Diffraction Grating Physics. https://www.newport.com/n/diffraction-grating-physics, Accessed at 10.06.2024.

[12] F. J. Eckle, *Handbook of Vacuum Science and Technology*, D. M. Hoffman, B. Singh, J. H. Thomas, J. H. Thomas, eds. (Academic Press, San Diego, 1998), chap. 2.2 - Diaphragm Pumps, pp. 84–96.

[13] Pfeiffer, Working with Turbopumps - Introduction to high and ultra high vacuum production. https://mmrc.caltech.edu/Vacuum/Pfeiffer%20Turbo/Turbos.pdf, Accessed at 18.06.2024.

[14] Pfeiffer, 4.3.2 Application. https://know-how-book.pfeiffer-vacuum.com/en/vacuum-generation/diaphragm-vacuum-pumps/application/index.html, Accessed at 18.06.2024.

[15] H. Henning, *Handbook of Vacuum Science and Technology*, D. M. Hoffman, B. Singh, J. H. Thomas, J. H. Thomas, eds. (Academic Press, San Diego, 1998), chap. 2.6 - Turbomolecular Pumps, pp. 183–213.

[16] Hamamatsu, VUV-MPPC 4th generation (VUV4). https://wiki.nikhef.nl/vuv/images/7/73/KSX-I50133-E_VUV-MPPC_b.pdf, Accessed at 21.06.2024.

[17] W. Zheng, L. Jia, F. Huang, Vacuum-ultraviolet photon detections, *iScience* **23**, 101145 (2020).

[18] R. A. Shukla, *et al.*, *2016 3rd International Conference on Emerging Electronics (ICEE)* (IEEE, 2016), pp. 1–4. Design and simulation of silicon photo-multiplier.

[19] Y. Musienko, Advances in multipixel geiger-mode avalanche photodiodes (silicon photomultiplies), *Nuclear Instruments and Methods in Physics Research Section A: Accelerators, Spectrometers, Detectors and Associated Equipment* **598**, 213 (2009).

[20] P. Windischhofer, W. Riegler, Passive quenching, signal shapes, and space charge effects in spads and sipms, *Nuclear Instruments and Methods in Physics Research Section A: Accelerators, Spectrometers, Detectors and Associated Equipment* **1045** (2023).

[21] VUV group Nikhef, Dark count dependence on temperature. https://wiki.nikhef.nl/vuv/Dark_count_dependence_on_temperature, Accessed at 21.06.2024.

[22] Pfeiffer, Operating Instructions MPT 200. https://wiki.nikhef.nl/vuv/images/4/44/Pg0025ben_c.pdf, Accessed at 09.06.2024.

[23] Pfeiffer, 5.1.2 Indirect, gas-dependent pressure measurement. https://know-how-book.pfeiffer-vacuum.com/en/vacuum-measuring-equipment/fundamentals-of-total-pressure-measurement/indirect-gas-dependent-pressure-measurement/index.html, Accessed at 17.06.2024.

[24] J. Mo, *et al.*, Surface-micromachined silicon carbide pirani gauges for harsh environments, *Nuclear Instruments and Methods in Physics Research Section A: Accelerators, Spectrometers, Detectors and Associated Equipment* **21**, 1350 (2021).

[25] G. K. T. Conn, H. N. Daglish, Cold cathode ionisation gauges for the measurement of low pressures, *Vacuum* **3**, 24 (1953).

[26] J. Priest, *Encyclopedia of Energy*, C. J. Cleveland, ed. (Elsevier, New York, 2004), chap. Temperature and Its Measurement, pp. 45–54.

[27] Heraeus Nexensos, Heraeus Nexensos 1 Pt100KN 1510 E Datasheet EN. https://www.mouser.com/datasheet/2/619/Pt100_KN1510E_TC3916_ceramic_wirewound_RTD_element-1760955.pdf, Accessed at 09.06.2024.

[28] Dracal Technologies, What Is a Pt100 RTD Sensor? https://www.dracal.com/en/what-is-a-pt100-rtd-sensor/#:~:text=In%20the%20case%20of%20a,A%2C%20B%2C%20or%20C., Accessed at 09.06.2024.

[29] D. V. Schroeder, *An introduction to thermal physics* (Oxford University Press, New York, 2021).

A Appendix of section 4

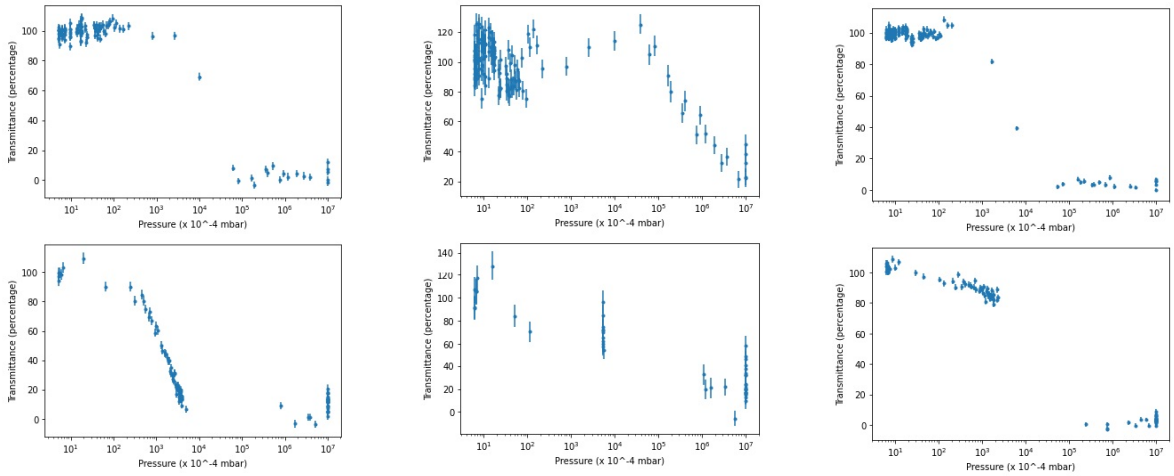

(a) wavelength = 128 nm (b) wavelength = 178 nm (c) wavelength = 140 nm

Figure 16: The transmittance of light with wavelengths of 128 nm, 178 nm and 140 nm as a function of pressure. The graphs are split in the data when the vacuum pump is turned on (top graph) and off (bottom graph).